TWO ORIGINS OF DUNITES IN THE NEW CALEDONIA OPHIOLITES: MELT-ROCK REACTION VERSUS FRACTIONAL CRYSTALLIZATION

Yang Xu[*,✉] and **Chuan-Zhou Liu**[*,**,***]

* *Laoshan Laboratory, Qingdao, China.*
** *State Key Laboratory of Lithospheric Evolution, Institute of Geology and Geophysics, Chinese Academy of Sciences, Beijing, China.*
*** *College of Earth and Planetary Sciences, University of Chinese Academy of Sciences, Beijing, China.*
✉ *Corresponding author, e-mail: Geoxuy@126.com*

Keywords: *Dunite; New Caledonia ophiolite; Geochemistry; Melt-rock reaction; Cumulate.*

ABSTRACT

Ophiolitic dunites offer critical insights into mantle and crustal processes within oceanic lithosphere. This study presents an integrated petrological and geochemical investigation of dunites from the New Caledonia ophiolite (Peridotite Nappe), a forearc lithospheric remnant. Two distinct dunite types with contrasting origins are identified. Type I dunites are crustal cumulates formed by fractional crystallization of primitive magmas. They occur at the base of the crustal ultramafic sequence with sharp contacts against pyroxenite layers, display a medium- to coarse-grained granular texture characterized by olivine grains forming triple junctions (~120°), and contain olivine with low Fo and spinel with low Cr#. Their mineral compositions follow fractional crystallization trends. Type II dunites are mantle-derived replacive bodies formed by melt-rock reaction between silica-undersaturated melts and harzburgite. They occur as veins or lenses within harzburgites with irregular contacts, exhibit granular to porphyroclastic textures with spinel forming "holly-leaf" or vermicular shapes commonly intergrown with orthopyroxene, and are characterized by extremely high olivine Fo and spinel Cr#. Geochemical data indicate that the two types likely formed during separate magmatic events. Furthermore, postcumulus infiltration of boninite-like melts into Type I dunites is evidenced by clinopyroxene with higher Mg# than coexisting olivine. The coexistence of these two dunite types underscores multiple magmatic processes in the formation of the New Caledonia ophiolite, involving both melt migration and crystal accumulation from depleted mantle-derived magmas.

INTRODUCTION

Ophiolites represent remnants of ancient oceanic lithosphere emplaced onto continents (e.g., Gass, 1968; Dewey and Bird, 1971; Moores and Vine, 1971; Dilek and Furnes, 2014). They are composed of both lithospheric mantle and oceanic crust (e.g., Anonymous, 1972; Escartín and Canales, 2011). The mantle section is predominantly composed of harzburgite and lherzolite, with minor dunite and pyroxenite, which can be variable serpentinized. The crustal section consists of a lower crust formed by cumulate rocks and an upper crust represented by mid-ocean ridge basalts (MORB). Near the crust-mantle transition zone at the base of the lower crust, ultramafic cumulates such as dunite, pyroxenite, and wehrlite are commonly present. Thus, dunite is a rock type found in both the mantle and crustal sections. It can record mantle processes, including partial melting and melt-rock reaction (e.g., Braun and Kelemen, 2002; Suhr et al., 2003; Zhou et al., 2005; Sanfilippo et al., 2017; Xiong et al., 2017, 2020; Basch et al., 2019; Rollinson, 2019; Zhou et al., 2021), as well as reflect the nature and origin of primitive magmas forming the oceanic crust (e.g., Pirard et al., 2013; Saccani and Tassinari, 2015; Borghini et al., 2018), providing key information for deciphering the evolution of oceanic lithosphere.

In this study, we focus on the New Caledonia ophiolite (Peridotite Nappe, Avias, 1967) in the southwest Pacific, which is considered a lithospheric relic formed in a forearc setting of an oceanic island arc (e.g., Prinzhofer and Allègre, 1985; Aitchison et al., 1995; Cluzel et al., 2001; Marchesi et al., 2009; Pirard et al., 2013; Secchiari et al., 2020; Xu and Liu, 2019; Xu et al., 2021, 2024). We conducted an integrated petrological and geochemical investigation of the dunites within this ophiolite. Our results indicate that the genesis of the New Caledonia ophiolitic dunites can be attributed to two distinct mechanisms, corresponding to key magmatic processes in the mantle and crust, respectively.

The first mechanism is melt-rock reaction. During percolation of silicaundersaturated melts through mantle peridotite (predominantly harzburgite), extensive dissolution-precipitation reactions occur between the melt and wallrock. This process leads to pyroxene dissolution and olivine precipitation, forming replacive dunites. Diagnostic features of such dunites include anomalously high spinel Cr# and olivine Fo values, and mineral compositions that deviate from partialmelting trends. These dunites are interpreted as fossil meltmigration channels within the mantle (e.g., Kelemen et al., 1995; Liang et al., 2011; Xiong et al., 2020; Zhou et al., 2021). The second mechanism is fractional crystallization, which operates in deep crustal magma chambers. Primitive highMg magmas ascend and accumulate in magma chamb ers, where olivine crystallizes as the dominant liquidus phase. Gravitational settling and accumulation of these crystals result in the formation of cumulate dunites. Such dunites display typical cumulate textures (e.g., equigranular, triplejunction structures), and their mineral compositions (e.g., olivine Fo and NiO contents, spinel TiO_2 content) follow welldefined fractionalcrystallization trends (e.g., Su et al., 2016; Borghini et al., 2018). In summary, the New Caledonia ophiolitic dunites provide key insights into melt migration, melt-rock reaction and fractional crystallization processes, offering a valuable window into the formation and modification of oceanic lithosphere in a forearc setting.

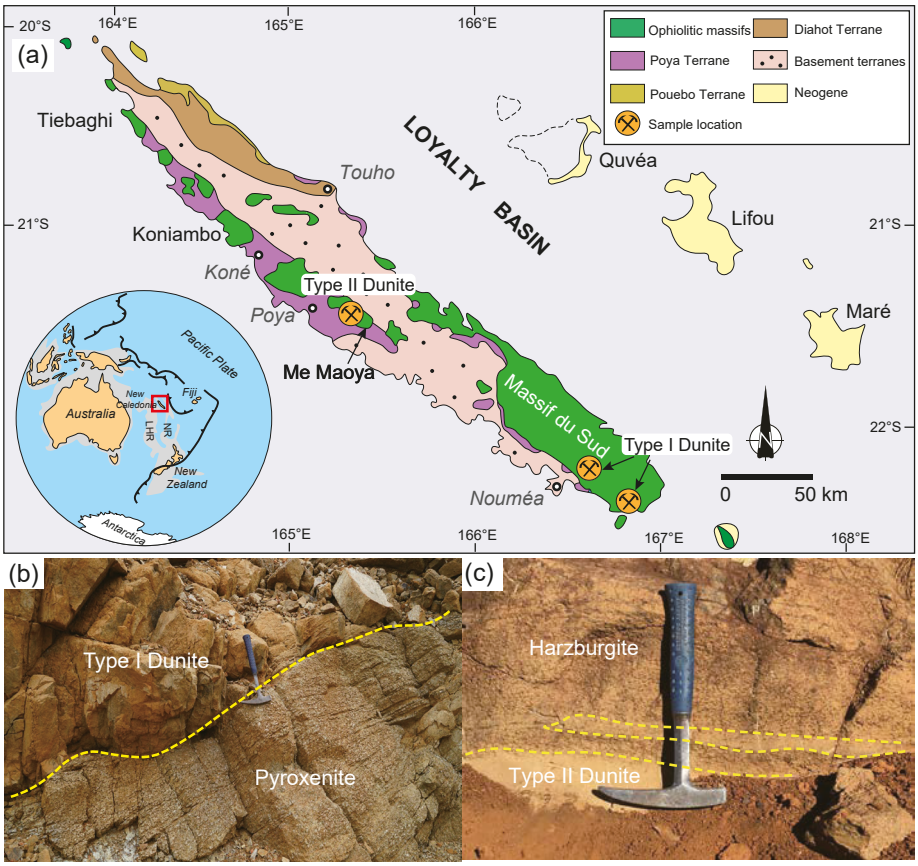

Fig. 1 - (a) Simplified geological map of New Caledonia, showing the distribution of major tectonic units and sample locations. (b, c) Representative field photographs of dunites from the New Caledonia ophiolite.

GEOLOGICAL SETTING

New Caledonia is situated in the southwestern Pacific Ocean (Fig. 1a) and represents a continental fragment that rifted from the eastern margin of Gondwana during the Late Cretaceous (Aitchison et al., 1995). The island consists of a complex assemblage of four major tectonic units: pre-Cretaceous basement terranes, a high-pressure-low-temperature (HP-LT) metamorphic belt, the Poya Terrane, and the ophiolitic massifs (Aitchison et al., 1995; Cluzel et al., 2001).

The pre-Cretaceous basement consists of Permian-Early Cretaceous arc-derived volcanic and sedimentary sequences accreted along the Australian margin (Cluzel et al., 2001). Overlying it, the Poya Terrane, structurally between the basement and Peridotite Nappe, comprises Poya basalts and Kone sediments intruded by dolerite sills. In northeastern New Caledonia, a Late Cretaceous-Eocene HP-LT metamorphic belt includes the Diahot and Pouebo terranes (Cluzel et al., 2001). The Diahot Terrane contains interlayered meta-sedimentary and volcanic rocks metamorphosed at ~550°C and 1.7 GPa (Fitzherbert et al., 2005), while the Pouebo Terrane is a subduction mélange with mafic blocks in a meta-serpentinite matrix. These mafic blocks resemble Poya E-MORB and experienced higher P-T conditions (~650°C, ~2.4 GPa; Clarke et al., 1997).

The Peridotite Nappe forms a large allochthonous ophiolitic unit (Avias, 1967), dominated by extensive peridotite massifs such as the Massif du Sud, Me Maoya, Koniambo, and Tiebaghi (Fig. 1a). These massifs have undergone significant erosion and/or tectonic detachment during ophiolite emplacement (Cluzel et al., 2001). The Massif du Sud, the largest of these (covering ~6000 km^2) and dominating the southern part of the island, locally exposes lower crustal cumulates, including dunites, wehrlites, olivine-bearing pyroxenites, and gabbronorites. Peridotites in New Caledonia are typically strongly serpentinized and affected by supergene weathering, although relatively fresh peridotites are locally preserved. Gabbroic and plagiogranitic dikes also intrude the peridotites, occasionally forming swarms of randomly oriented, cross-cutting veinlets. Geochemical data suggest that these mafic and felsic intrusions are related to subduction-related magmatism (Cluzel et al., 2006, 2024). Zircon U-Pb dating indicates Early Eocene emplacement ages (~50-55 Ma) for both gabbro and plagiogranite intrusions (Cluzel et al., 2006, 2016; Xu et al., 2022b; Cluzel et al., 2024). Beneath the peridotite massifs, high-temperature amphibolite lenses are interpreted as remnants of a metamorphic sole. Hornblende from these lenses yields an $^{40}Ar/^{39}Ar$ age of 55.4 ± 1.0 Ma, consistent with a zircon U-Pb age of 54.66 ± 0.83 Ma, recording subduction initiation near a spreading ridge (Cluzel et al., 2012).

SAMPLE DESCRIPTIONS

This study investigates fourteen dunite samples collected from the Massif du Sud and the Me Maoya massif (Fig. 1a). Based on field occurrence, these dunites can be subdivided into two types: Type I and Type II.

Type I dunites occur at the base of the crustal ultramafic sequence in the Massif du Sud, typically showing sharp contacts with pyroxenite layers (Fig. 1b). These rocks have undergone weak serpentinization, in which olivine commonly exhibits mesh texture and is replaced or crosscut by serpentine veins (Fig. 2). The samples display a medium- to coarse-grained granular texture (1-8 mm), with olivine grains forming triple junctions approaching 120° (Fig. 2a). Primary

orthopyroxene is absent in Type I dunites. Clinopyroxene is typically associated with spinel and shows orthopyroxene exsolution lamellae (Fig. 2d, f). Discrete spinel grains generally show subrounded morphologies (Fig. 2e).

Type II dunites occur as veins or lenses within harzburgites of the Me Maoya massif (Fig. 1c). Ranging in thickness from 1 to 10 cm, they show irregular contacts with the host harzburgites. In contrast to Type I, Type II dunites are significantly fresher (Fig. 2b) and show granular to porphyroclastic textures (Fig. 2b). They are predominantly composed of olivine (>95 vol. %) with minor orthopyroxene (<5 vol. %). Olivine commonly contains kink bands (Fig. 2b). Spi-

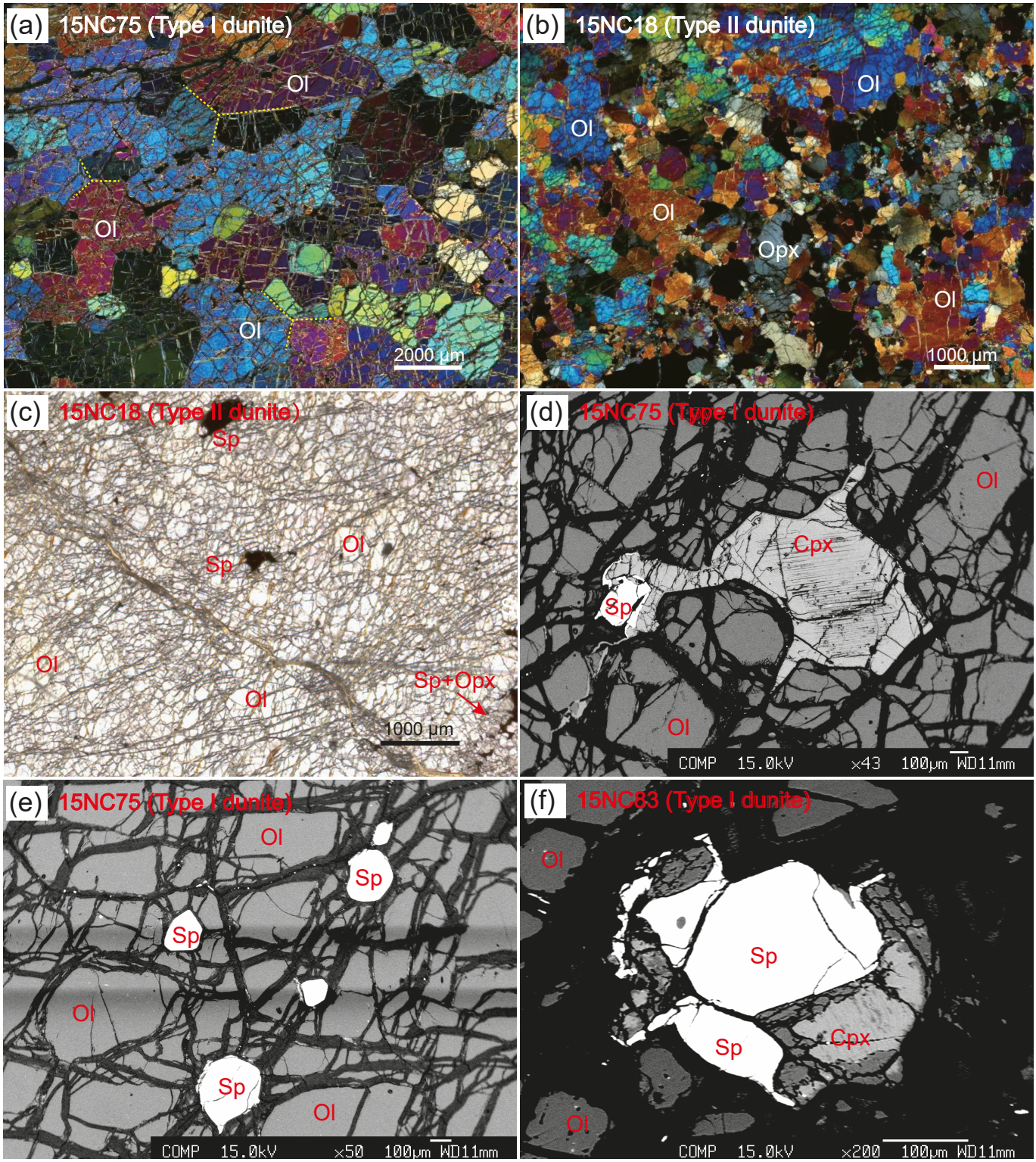

Fig. 2 - Microtextures of New Caledonia dunites. (a) Type I dunite exhibiting a medium- to coarse-grained granular texture. (b) Type II dunite displaying granular to porphyroclastic textures. (c) Large holly-leaf shaped spinel grains and smaller spinel associated with orthopyroxene in a Type II dunite. (d-f) Backscattered electron (BSE) images of Type I dunites. Olivine grains are commonly fractured and show mesh textures due to serpentinization. Spinel is found both as grains intergrown with clinopyroxene and as discrete grains disseminated in olivine. Ol, olivine; Sp, spinel; Opx, orthopyroxene; Cpx, clinopyroxene.

nel occurs either as individual grains or as symplectitic intergrowths with orthopyroxene (Fig. 2c), a texture that is similar to those previously described in New Caledonia harzburgites (Secchiari et al., 2019; Xu et al., 2021). Larger spinel grains typically exhibit "holly-leaf" or lobate shapes, while smaller, irregularly shaped grains are often disseminated among orthopyroxene and olivine (Fig. 2c).

Mineral modes were determined through mass-balance calculations based on whole-rock and mineral major-element compositions (Table 1). Volume fractions were derived from weight fractions by applying density ratios of 1.03 for clinopyroxene/olivine, 0.97 for orthopyroxene/olivine, and 1.1 for spinel/olivine (Le Roux et al., 2014). Type I dunites consist of 89.5-98.0 vol% olivine, 1.4-8.8 vol% spinel, and minor clinopyroxene (≤3.5 vol%). In comparison, Type II dunites exhibit higher olivine contents (96.3-99.9 vol%) and lower spinel contents (0.1-1.2 vol%).

ANALYTICAL METHODS

Prior to analysis, altered rock rims were carefully removed. The samples were crushed into small fragments using a rock hammer between thick plastic sheets. Fresh pieces were selected and ground to a fine powder of ~200 mesh in an agate mill. All analytical work was conducted at the Institute of Geology and Geophysics, Chinese Academy of Sciences (IGGCAS).

Whole-Rock and Mineral Major Elements

Whole-rock major element compositions were determined by X-ray fluorescence (XRF) spectroscopy. Approximately 0.5 g of sample powder was mixed with 5 g of $Li_2B_4O_7$ and fused into glass beads, which were analyzed using an AXIOS Mineral spectrometer. Analytical uncertainties range from 1% to 3%. Loss on ignition (LOI) was determined from the weight difference after calcination at 1000 °C.

Major element compositions of minerals were analyzed by wavelength-dispersive spectrometry (WDS) using a JEOL JXA-8100 electron microprobe, operating at an accelerating voltage of 20 kV and a beam current of 20 nA. Natural minerals and synthetic oxides were used as standards, and matrix corrections were applied using the ZAF procedure. Analytical uncertainty is ≤1.5%.

Clinopyroxene trace element composition

In situ trace element analyses of clinopyroxene in sample 15NC71 were performed by laser ablation inductively coupled plasma mass spectrometry (LA-ICP-MS), employing a GeoLas HD 193 nm ArF excimer laser ablation system coupled to a Thermo Element XR high resolution ICP-MS. Measurements were conducted in peak-hopping mode. Two to four spots were analyzed on different pyroxene grains using an 80 μm spot size and a repetition rate of 8 Hz. The NIST 610 glass was used as the external calibration standard, and NIST 614 was employed as a quality control monitor. Reference values for NIST 610 and 614 were obtained from the GeoREM database. Calcium was used as the internal standard. Data reduction was carried out using the GLITTER 4.0 software (Griffin et al., 2008). Precision for most trace elements in NIST 614 is better than 5%, while Zr, Tb, and Hf show precisions of 5-10%.

Table 1 - Whole-rock major element (in wt%) and modal compositions of the New Caledonia ophiolitic dunites.

Sample	15NC63	15NC64	15NC65	15NC73	15NC75	15NC83	15NC14	15NC16	15NC16R	15NC18	15NC19
Type	I	I	I	I	I	I	II	II	II	II	II
GPS	22°13'22" S, 166°39'38" E	22°13'22" S, 166°39'38" E	22°13'22" S, 166°39'38" E	22°12'39" S, 166°40'36" E	22°12'39" S, 166°40'36" E	22°20'28" S, 166°52'49" E	21°28'3" S, 165°23'40" E	21°28'3" S, 165°23'40" E	21°28'3" S, 165°23'40" E	21°28'3" S, 165°23'40" E	21°28'3" S, 165°23'40" E
SiO_2	38.25	38.78	38.30	38.77	37.82	34.50	37.06	37.78	37.95	40.72	41.11
TiO_2	0.01	0.00	0.01	0.01	0.01	0.02	0.01	0.02	0.01	0.00	0.00
Al_2O_3	1.11	0.42	0.51	0.49	0.35	1.61	0.00	0.06	0.11	0.14	0.00
TFe_2O_3	9.54	9.54	9.73	10.68	10.21	8.17	5.26	7.55	7.56	8.36	6.64
MnO	0.15	0.13	0.15	0.15	0.15	0.11	0.06	0.10	0.10	0.11	0.08
MgO	37.62	39.49	39.42	42.86	45.30	41.51	47.07	44.98	44.92	47.18	47.88
CaO	0.58	0.11	0.12	0.22	0.50	0.69	0.04	0.04	0.04	0.36	0.04
Na_2O	0.00	0.00	0.00	0.00	0.00	0.00	0.00	0.00	0.00	0.00	0.00
K_2O	0.01	0.01	0.01	0.01	0.01	0.02	0.00	0.00	0.00	0.00	0.00
Cr_2O_3	2.32	1.06	1.00	0.78	0.66	2.37	0.12	0.95	0.96	0.46	0.40
NiO	0.34	0.26	0.25	0.28	0.25	0.31	0.34	0.35	0.34	0.35	0.36
LOI	10.47	10.77	10.69	5.51	5.16	11.02	10.27	8.49	8.41	1.64	4.14
Total	100.40	100.58	100.20	99.77	100.41	100.32	100.23	100.32	100.40	99.32	100.65
Mg#	88.65	89.13	88.92	88.83	89.78	90.96	94.66	92.19	92.17	91.79	93.46
Mode(vol%)											
Ol	91.2	96.5	96.9	97.2	98.0	89.5	99.9	99.5	98.8	96.3	99.9
Cpx	0	0.1	0	0.4	0.6	3.5	0	0	0	0	0
Opx	0	0	0	0	0	0	0	0	0	2.9	0
Spl	8.8	3.4	3.1	2.4	1.4	7.0	0.1	0.5	1.2	0.8	0.1

TFe2O3: total iron oxide as ferric iron. LOI: loss on ignition. R: replicate analysis.

RESULTS AND DISCUSSION

The formation of lithospheric dunites is attributed to three primary mechanisms: high-degree partial melting of primitive mantle (e.g., Kubo, 2002; Beyer et al., 2006; Xie et al., 2013); melt-rock reaction between peridotite and silica-undersaturated melts (e.g., Braun and Kelemen, 2002; Suhr et al., 2003; Zhou et al., 2005; Sanfilippo et al., 2017; Xiong et al., 2017, 2020; Rollinson, 2019; Zhou et al., 2021); fractional crystallization of mafic magmas (e.g., Hattori et al., 2010; Pirard et al., 2013; Borghini et al., 2018).

Type I Dunite: Cumulate Products of Mafic Magma Crystallization

Type I dunites display a granular texture and show no significant deformation (Fig. 2a). They are commonly associated with pyroxenites and gabbronorites (Fig. 1b), forming layered or lenticular cumulate sequences (e.g., Pirard et al., 2013). The wholerock MgO, Al_2O_3 and CaO contents of Type I dunites vary within ranges similar to those of New Caledonia harzburgites, but their SiO_2 contents are systematically lower (Fig. 3). In MgO vs. SiO_2 diagrams (Fig. 3), Type I dunites plot below the mantle melting trend. Furthermore, wholerock Mg# values of Type I dunites range from 88.65 to 90.96 (average 89.38; Table 1), which are distinctly lower than those of New Caledonia harzburgites that typically exhibit Mg# >91 (Marchesi et al., 2009; Ulrich et al., 2010; Liu et al., 2018; Secchiari et al. 2020). These features preclude a residual origin for Type I dunites after highdegree mantle melting.

In terms of mineral chemistry, these dunites fall outside the olivine-spinel mantle array (OSMA; Arai, 1994) in a spinel Cr# vs. olivine Fo diagram (Fig. 4). Their olivines have lower Fo values than those in New Caledonia harzburgites (Fig. 4). In the diagram of olivine Fo vs. NiO, Type I dunites deviate from the mantle trend and show lower NiO contents than harzburgites, resembling compositions reported for cumulate dunites (Fig. 5a, Su et al., 2016). Olivine Fo correlates positively with NiO but negatively with CaO and MnO, consistent with compatible behavior of Ni and incompatible behavior of Ca and Mn in olivine during fractional crystal-

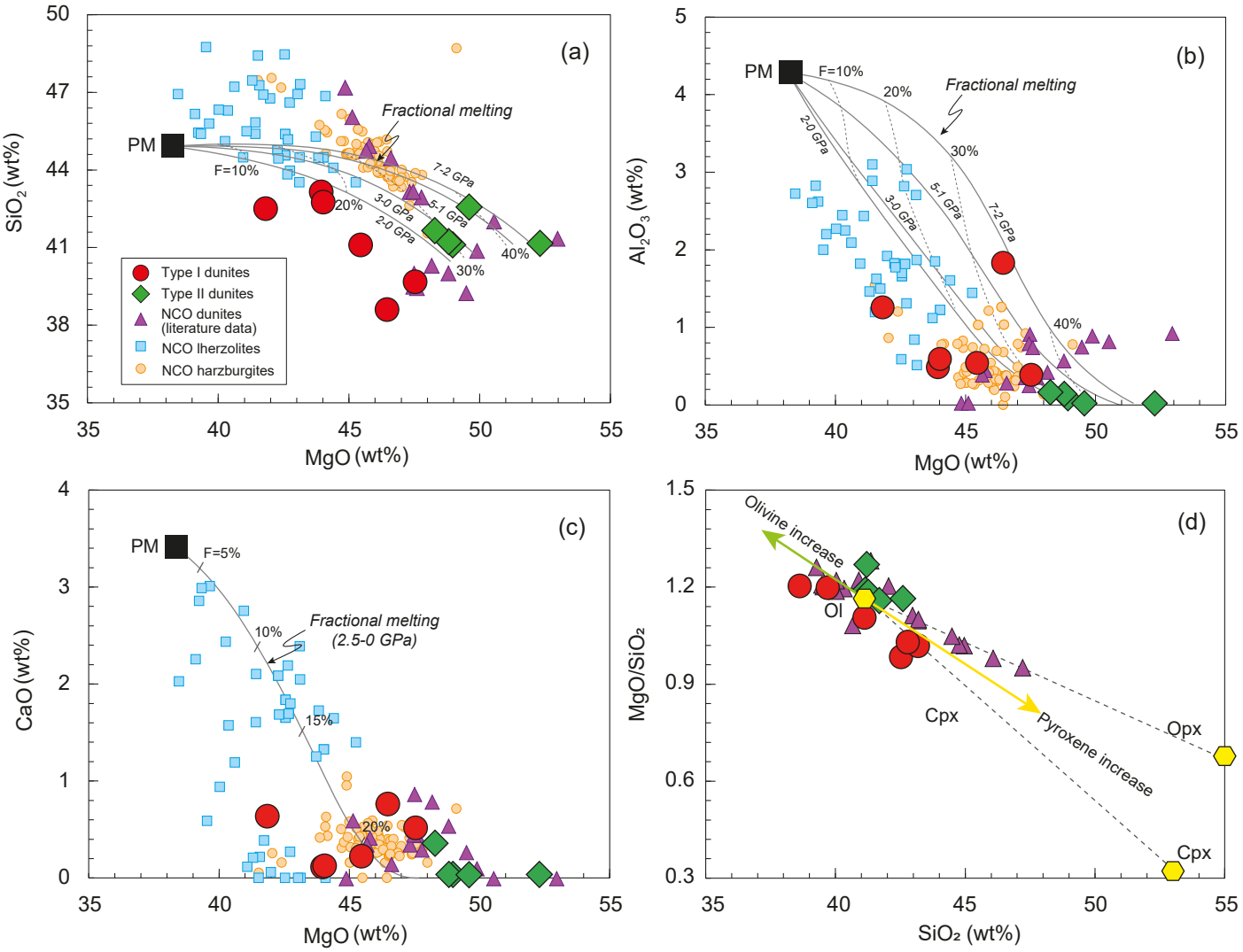

Fig. 3 - Whole rock major element compositions of New Caledonia dunites. MgO vs. SiO_2 (a), Al_2O_3 (b), CaO (c), and SiO_2 vs MgO/SiO_2 (d). The polybaric fractional melting curves in (a) and (b) are from Herzberg, 2004. In (c) trend of fractional melting at 2.5-0 GPa are from Niu (1997). Mixing lines for Ol-Opx and Ol-Cpx are from Saka et al. (2014) and Walter (1998), respectively. Literature data for New Caledonia peridotites are from Marchesi et al. (2009), Ulrich et al. (2010), Secchiari et al. (2016, 2020), Liu et al. (2018), and Xu et al. (2022a).

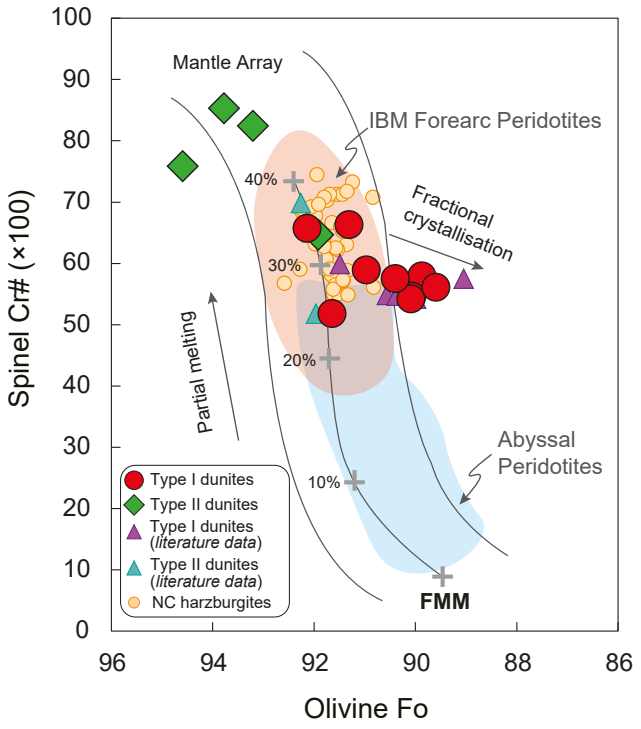

lization (Fig. 5a-c). Chromium is a major element in spinel, and studies indicate that Crrich spinel typically crystallizes near the liquidus, either simultaneously with or shortly after olivine (Ulmer et al., 2018). This can explain the relationship between olivine Fo and Cr content in Type I dunites (Fig. 5d): if Crspinel saturation slightly lags olivine crystallization, olivine Fo and Cr display a negative correlation; if both phases crystallize concurrently, a weak positive or scattered correlation is expected. Compared to harzburgites, spinel in Type I dunites has lower Cr# but higher MnO, while their NiO contents largely overlap (Fig. 6). Notably, despite having low Cr#, these spinels contain anomalously high TiO_2 (Fig. 6d), supporting post-formation melt infiltration as a key process affecting the Type I dunites.

Fig. 4 - Spinel Cr# vs. olivine Fo for New Caledonia dunites. The Olivine-Spinel Mantle Array (OSMA) is from Arai (1994). Data for abyssal peridotites (Warren, 2016; Xu et al., 2025), Izu-Bonin-Mariana (IBM) forearc peridotites (Parkinson and Pearce, 1998), and New Caledonia harzburgites (Pirard et al., 2013; Secchiari et al., 2020; Xu et al., 2021) are shown for comparison.

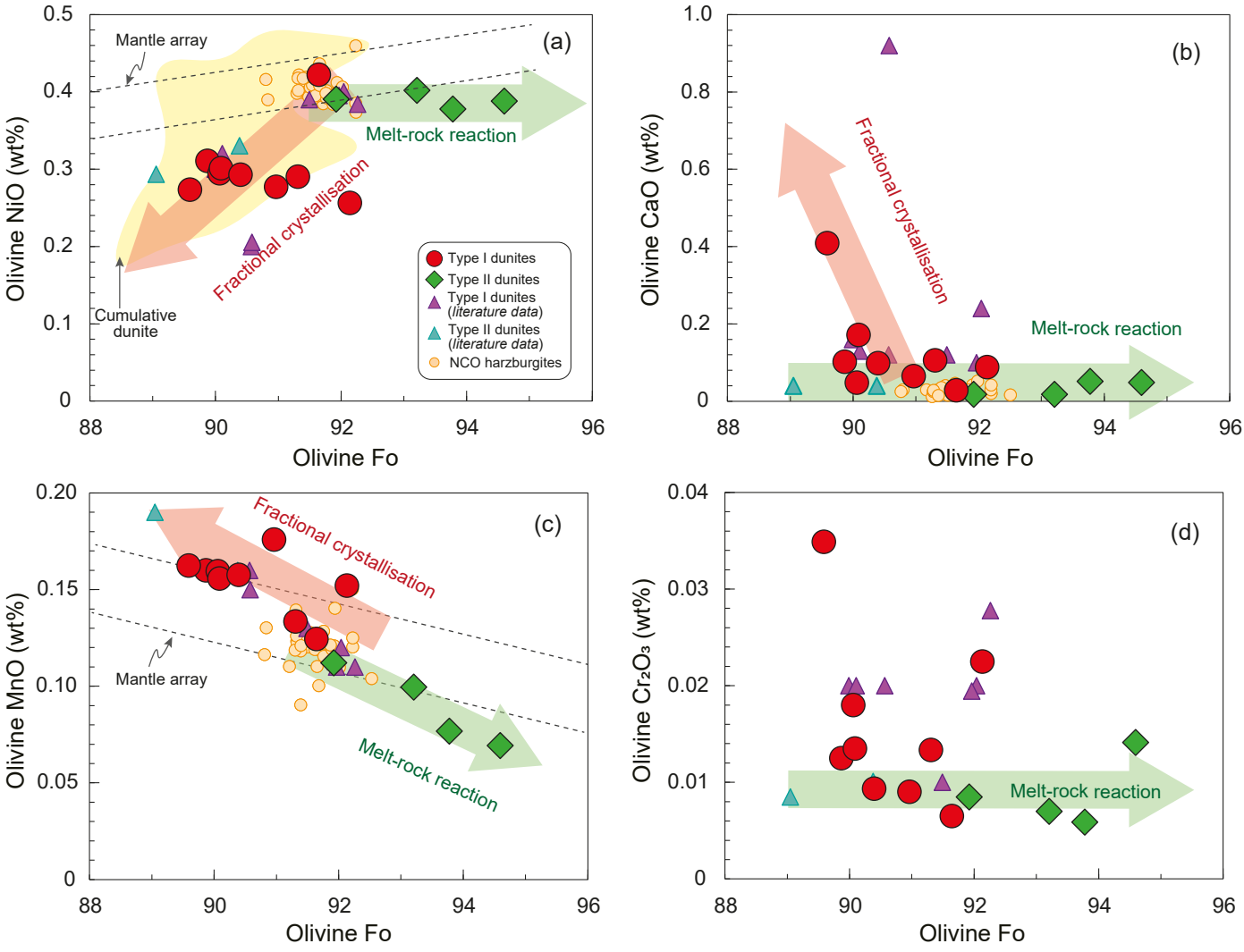

Fig. 5 - Olivine major element compositions. Olivine Fo vs. NiO (a), CaO (b), MnO (c), and Cr_2O_3 (d). Fields for cumulative dunites are from Su et al. (2016). Mantle array references are from Ozawa (1994). Data sources are the same as in Fig. 4.

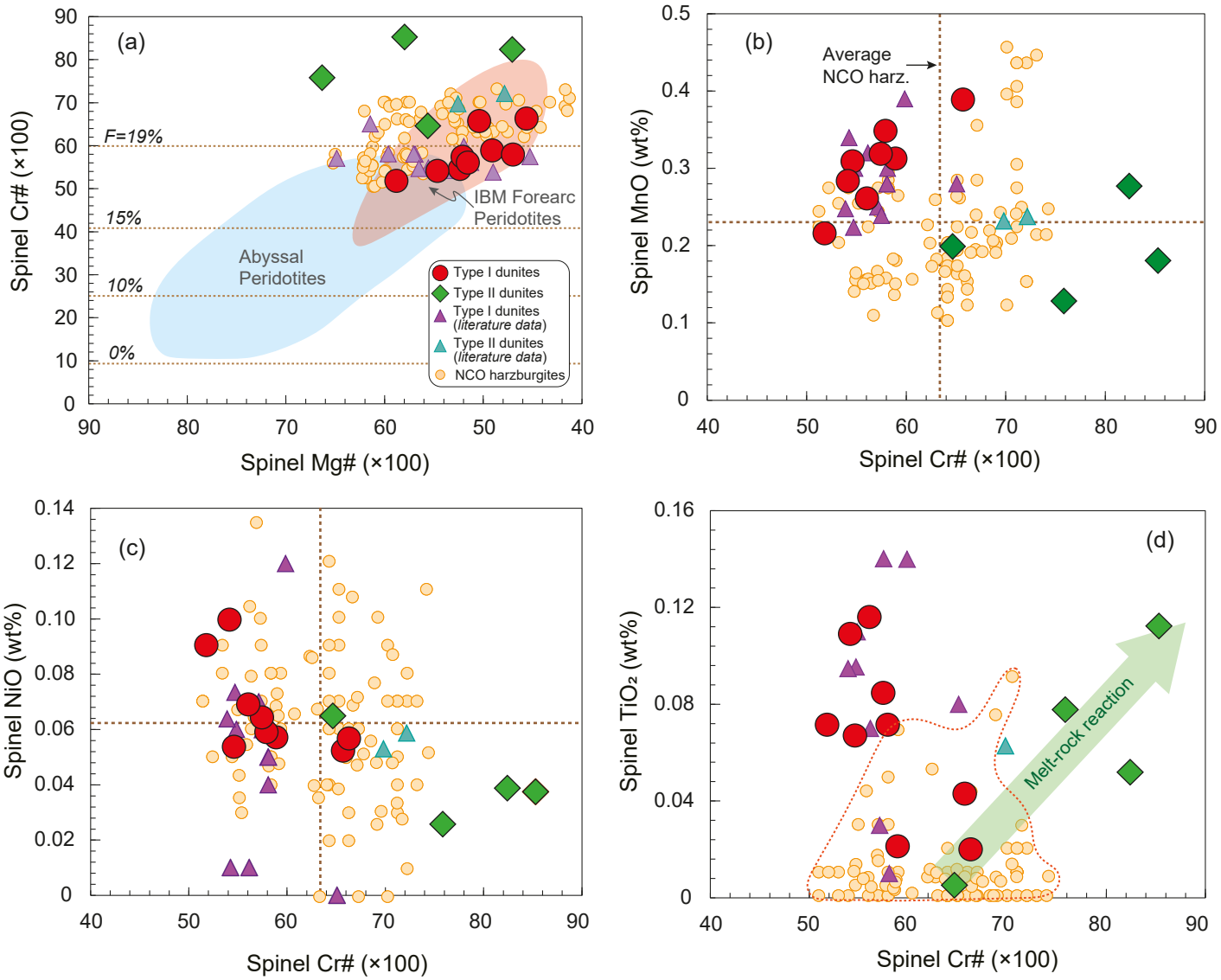

Fig. 6 - Spinel major element compositions. Spinel Cr# vs Mg# (a), MnO (b), NiO (c), and TiO_2 (d). Data sources are the same as Fig. 4.

Type-II Dunite: Evidence of Melt-rock Reaction

Type II dunites share textural similarities with their harzburgitic wall-rocks, exhibiting a porphyroclastic texture that evolved into a granular fabric through syntectonic recrystallization (e.g., Pirard et al., 2013; Xu et al., 2021). Unlike the rounded, subidiomorphic spinel grains common in Type I dunites (Fig. 2e), spinel in Type II dunites often shows vermicular overgrowth textures. Such textures are typically interpreted as resulting from the percolation of orthopyroxene-undersaturated melts (Kelemen et al., 1990; Pirard et al., 2013).

Geochemically, Type II dunites are characterized by lower wholerock Al_2O_3 and CaO (Fig. 3; Table 1), lower spinel MnO and NiO (Fig. 6; Table 2), but higher olivine Fo and spinel Cr# compared to Type I (Fig. 4; Table 3). Olivine Fo shows no systematic correlation with NiO, CaO, or Cr_2O_3 (Fig. 5), inconsistent with an origin via partial melting or fractional crystallization. Spinel composition is a sensitive indicator of melt extraction, as Al and Mg are preferentially partitioned into the melt relative to Cr and Fe, leading to increasing Cr# and decreasing Mg# during melting (Dick and Bullen, 1984). However, Type II dunite spinels show no clear correlation between Cr# and Mg# (Fig. 6a). Their exceptionally high Cr# values (0.64-0.85), significantly exceeding those of New Caledonia harzburgites (Fig. 6a), cannot be explained by mantle melting alone. Instead, such compositions are characteristic of dunite veins with abyssal and ophiolitic peridotites (e.g., Dare et al., 2009; Arai et al., 2011; Warren, 2016; Xiong et al., 2017; Zhou et al., 2021; Zhang et al., 2023). These dunite veins are widely regarded as reactive melt channels within mantle peridotite (e.g., Kelemen et al., 1995; Liang et al., 2011; Xiong et al., 2020; Zhou et al., 2021). The high Cr# signature likely reflects Al extraction from spinel into the melt during meltrock reaction, while Cr is retained and enriched due to its strong compatibility in spinel. In suprasubduction zone (SSZ) settings, dunite veins commonly exhibit very high spinel Cr#, attributed to reaction between boninitic melts and mantle peridotite (Dare et al., 2009; Arai et al., 2011; Pearce et al., 2019; Bilici, 2022). This interpretation is further supported by a positive correlation between spinel Cr# and TiO_2 in Type II dunites (Fig. 6d), since spinel strongly incorporates Ti during meltrock interaction, lead-

Table 2 - Representative major element (in wt%) compositions of spinel.

Sample	Type	n	SiO_2	TiO_2	Al_2O_3	Cr_2O_3	FeO	MnO	MgO	CaO	Na_2O	NiO	Total	Mg#	Cr#
15NC63	I	8	0.06	0.04	17.54	50.09	20.03	0.39	11.42	0.01	0.03	0.05	99.66	50.4	65.7
15NC64	I	4	0.02	0.02	16.99	49.81	22.23		10.46	0.38	0.01	0.06	99.98	45.6	66.3
15NC65	I	7	0.04	0.02	21.19	45.30	21.22	0.31	11.48	0.00	0.02	0.06	99.64	49.1	58.9
15NC71-2	I	4	0.04	0.07	22.00	45.14	21.21	0.35	10.54	0.10	0.01	0.06	99.51	47.0	57.9
15NC72	I	6	0.07	0.07	24.87	44.62	19.06	0.31	11.76	0.22	0.04	0.05	101.06	52.4	54.6
15NC73	I	4	0.03	0.11	24.02	42.27	19.36	0.28	13.09	0.01	0.01	0.10	99.27	54.6	54.1
15NC74	I	8	0.06	0.08	22.20	44.69	19.93	0.32	12.16	0.01	0.00	0.06	99.51	52.1	57.5
15NC75	I	6	0.06	0.12	23.06	43.87	20.20	0.26	12.06	0.01	0.04	0.07	99.75	51.6	56.1
15NC83	I	8	0.02	0.07	26.63	42.66	16.86	0.22	13.49	0.01	0.01	0.09	100.05	58.8	51.8
15NC16	II	8	0.05	0.05	8.82	61.52	19.62	0.28	9.78	0.01	0.02	0.04	100.20	47.0	82.4
15NC18	II	8	0.05	0.01	18.80	51.26	17.40	0.20	12.23	0.01	0.02	0.06	100.03	55.6	64.7
15NC19	II	8	0.04	0.11	7.55	65.34	15.33	0.18	11.86	0.00	0.01	0.04	100.47	58.0	85.3
15NC14	II	8	0.03	0.08	12.98	60.76	12.60	0.13	13.92	0.01	0.01	0.03	100.53	66.3	75.8

Table 3 - Representative major element (in wt%) compositions of olivine.

Sample	Type	n	SiO_2	TiO_2	Al_2O_3	Cr_2O_3	FeO	MnO	MgO	CaO	Na_2O	NiO	Total	Fo
15NC63	I	8	41.32	0.02	0.00	0.02	7.79	0.15	51.24	0.09	0.01	0.26	100.90	92.1
15NC64	I	4	41.06	0.00	0.00	0.01	8.57	0.13	50.54	0.11	0.01	0.29	100.72	91.3
15NC65	I	6	41.25	0.01	0.02	0.01	8.74	0.18	49.39	0.06	0.00	0.28	99.93	91.0
15NC71-2	I	8	40.58	0.01	0.00	0.01	9.88	0.16	49.18	0.10	0.01	0.31	100.24	89.9
15NC72	I	5	40.61	0.01	0.00	0.02	9.67	0.16	49.18	0.05	0.02	0.29	100.01	90.1
15NC73	I	4	40.63	0.00	0.01	0.01	9.68	0.16	49.36	0.17	0.00	0.30	100.31	90.1
15NC74	I	4	40.86	0.01	0.02	0.01	9.42	0.16	49.75	0.10	0.00	0.29	100.61	90.4
15NC75	I	8	40.62	0.02	0.05	0.03	9.99	0.16	48.26	0.41	0.03	0.27	99.84	89.6
15NC83	I	8	41.20	0.00	0.03	0.01	8.15	0.12	50.18	0.03	0.01	0.42	100.15	91.6
15NC16	II	8	41.66	0.01	0.03	0.01	6.66	0.10	51.29	0.02	0.00	0.40	100.18	93.2
15NC18	II	8	41.07	0.02	0.01	0.01	7.84	0.11	50.08	0.02	0.01	0.39	99.55	91.9
15NC19	II	8	41.64	0.00	0.01	0.01	6.09	0.08	51.47	0.05	0.00	0.38	99.73	93.8
15NC14	II	8	41.95	0.01	0.01	0.01	5.32	0.07	52.29	0.05	0.00	0.39	100.10	94.6

ing to TiO_2 enrichment (e.g., Dare et al., 2009; Pearce et al., 2019; Bilici, 2022). It is noteworthy that three Type II dunite samples have anomalously high olivine Fo, with one plotting outside the Mantle Array (Fig. 4). This is most likely a result of sub-solidus Fe^{2+}–Mg exchange between spinel and olivine (e.g., Barnes and Roeder, 2001). Moreover, Type II dunites do not follow a pyroxene-enrichment trend in whole-rock SiO_2 vs. MgO/SiO_2 diagrams (Fig. 3d), suggesting that the reaction involved pyroxene dissolution and olivine precipitation. We therefore conclude that Type II dunites formed by interaction between silica-undersaturated melts and peridotites.

Assuming that the two types of dunites in New Caledonia ophiolite originated from a common parental magma series, their formation process could be envisioned as follows: during subduction, melting of depleted mantle would produce high-temperature, high-Mg melts. These melts could first react with the mantle during ascent to form replacive (Type II) dunites, and subsequently accumulate in magma chambers, where fractional crystallization would give rise to cumulative (Type I) dunites. However, the geochemical characteristics of Type II dunites indicate that the melts involved in the melt-rock reaction were distinctly low in CaO and MnO but high in TiO_2 and Mg# (Table 1; Figs. 3, 5, 6), contrasting sharply with the primitive samples of Type I dunites, which show high CaO and MnO but low TiO_2 and Mg#. This suggests that the two dunite types may represent products of separate magmatic episodes. The coexistence of cumulate dunites with low spinel Cr# and reaction dunites with high spinel Cr#, formed by distinct magmatic events, is commonly observed in ophiolites (e.g., Xiong et al., 2017; Zhou et al., 2021).

Infiltration of high-Mg melts into the Type I dunites

Type I dunites are characterized by high modal olivine contents (>90%), suggesting crystallization from a primitive parental magma. However, clinopyroxene in these rocks displays interstitial textures (Fig. 2d, f) and contains elevated TiO_2 and Al_2O_3 (Fig. 7), which points to a metasomatic origin. Furthermore, these clinopyroxenes exhibit higher Mg# than coexisting olivine (Table 3, 4), possibly indicating that the dunites were infiltrated by high-Mg melts after their formation. This interpretation is based on two factors: first, during the crystallization of mafic magma, olivine typically forms earlier than clinopyroxene, causing the melt Mg# to decrease over time; thus, later-crystallizing clinopyroxene would normally have a lower Mg# than earlier olivine. Second, clinopyroxene has a higher FeMg partition coefficient ($K_D^{Fe\text{-}Mg} = [FeO^{mineral} \times MgO^{liq}] / [FeO^{liq} \times MgO^{mineral}]$) than olivine (~0.28-0.46 vs ~0.26-0.39; e.g., Roeder and Emslie, 1970; Kinzler, 1997), which can also lead to clinopyroxene Mg# values comparable to or even lower than those of olivine. In summary, the mineralogical and geochemical evidence supports the formation of clinopyroxene through post-cumulus melt infiltration after the establishment of the Type I dunite framework. This further implies that such cumulate dunites can subsequently act as permeable channels for migrating melts.

Clinopyroxene in this study shows positive correlations of Al_2O_3 with Cr_2O_3 and TiO_2, and of Mg# with CaO, but a negative correlation between Mg# and MnO (Fig. 7). Using the Fe-Mg distribution coefficients for clinopyroxene from Bédard (2010), the calculated Mg# values of melts in equilibrium with clinopyroxene in Type I dunites range from 74 to 82 (Table 4), comparable to those reported for boninites (e.g., Crawford et al., 1989; Pearce et al., 2019). Therefore, the high Mg# of clinopyroxene in Type I dunites could reflect infiltration by boninitic melts. A similar relationship has been documented in cumulate dunites from other ophiolites and peridotite massifs. For example, in the Bay of Islands Ophiolite, cumulate dunites yield olivine Mg# = 88.5-91.2 and clinopyroxene Mg# = 90.8-94.2 (Suhr et al., 1998). Similarly, in the Cabo Ortegal complex, cumulate dunites show olivine Mg# = 86.7-92.3 and clinopyroxene Mg# = 91.5-95.2 (Santos et al., 2002).

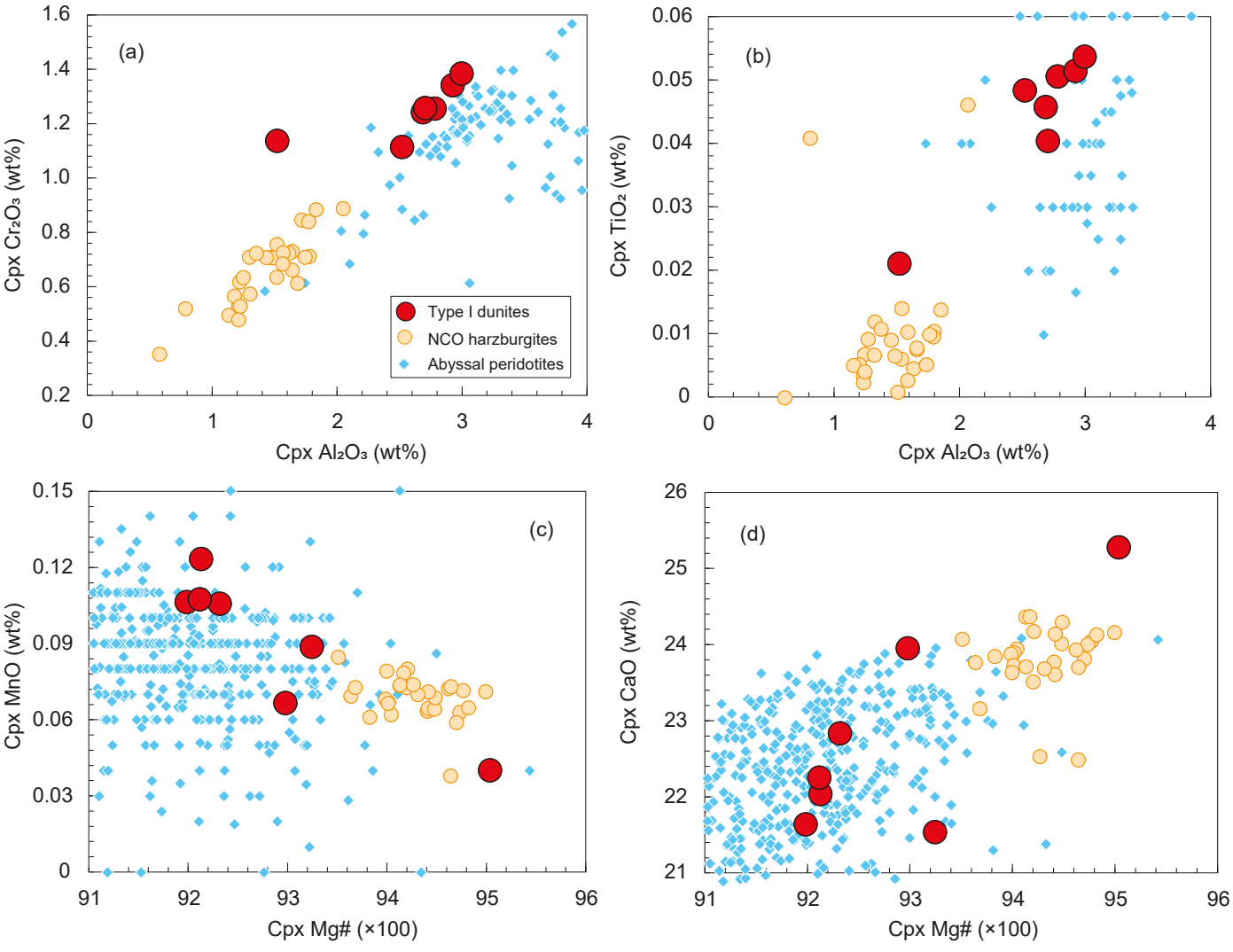

Fig. 7 - Clinopyroxene major element compositions. Cpx Al_2O_3 vs Cr_2O_3 (a) and TiO_2 (b), Cpx Mg# vs MnO (c) and CaO (d). Data sources are the same as Fig. 4.

Table 4 - Representative major element (in wt%) compositions of clinopyroxene.

Sample	Type	n	SiO_2	TiO_2	Al_2O_3	Cr_2O_3	FeO	MnO	MgO	CaO	Na_2O	NiO	Total	Mg#	EM Mg#
15NC64	I	8	52.52	0.02	1.52	1.14	1.63	0.04	17.46	25.28	0.01	0.05	99.66	95.0	82
15NC71-2	I	12	52.68	0.05	2.69	1.24	2.84	0.11	18.28	21.64	0.25	0.03	99.80	92.0	75
15NC72	I	6	53.09	0.05	2.52	1.11	2.75	0.12	18.09	22.03	0.21	0.03	100.02	92.1	75
15NC73	I	4	52.51	0.05	2.78	1.26	2.20	0.07	16.35	23.95	0.51	0.04	99.71	93.0	77
15NC74	I	8	52.76	0.04	2.70	1.26	2.62	0.11	17.67	22.83	0.27	0.04	100.30	92.3	76
15NC75	I	5	53.64	0.05	2.92	1.34	2.57	0.11	16.84	22.25	0.47	0.02	100.21	92.1	74
15NC83	I	8	53.75	0.05	3.00	1.38	2.30	0.09	17.78	21.53	0.49	0.04	100.42	93.2	78

*EM: equilibrium melt.

Clinopyroxenes in Type I dunites have lower rare earth element (REE) abundances than those in abyssal peridotites and pyroxenite veins within New Caledonia harzburgites (Fig. 8a, Table 5). The latter are thought to have crystallized from parental magmas of the New Caledonian CE-boninites (Xu et al., 2021). We further calculated the compositions of melts in equilibrium with clinopyroxene from Type I dunites. The inferred equilibrium melts show significantly lower trace element contents than N-MORB and CE-boninites, and exhibit pronounced negative Zr-Hf anomalies, contrasting with the slight positive Zr-Hf anomalies typical of boninites (Fig. 8b). In addition, the melts are enriched in Rb, Th, and Sr. Their trace element abundances and patterns resemble those of melts in equilibrium with New Caledonia gabbronorites (Secchiari et al., 2018; Fig. 8b). Thus, the melts that infiltrated the Type I dunites share a similar origin with the parental magma of New Caledonia gabbronorites, both being derived from moderate degrees of melting of a depleted, refractory mantle source (Secchiari et al., 2018). Nevertheless, notable differences are observed. The clinopyroxene-equilibrium melts exhibit higher abundances of fluid-mobile elements (such as Rb and Ba), implying a greater role for hydrous fluids. Additionally, their significantly higher Mg# (74-82 vs. 69-72) suggests that these melts were either derived from a more refractory mantle source or that the parental magmas of the gabbronorites underwent a greater degree of differentiation.

CONCLUSIONS

New Caledonia ophiolitic dunites originate via two distinct mechanisms: Type I dunites are crustal cumulates formed by fractional crystallization of primitive magmas, characterized by granular textures and mineral compositions following fractional crystallization trends; Type II dunites are mantle-derived replacive bodies formed by melt-rock reaction between silica-undersaturated melts and peridotite, distinguished by high olivine Fo, extremely high spinel Cr#, and vermicular spinel textures. Their contrasting geochemical signatures suggest formation from separate magmatic events rather than a common parental magma series. Furthermore, postformation melt infiltration is evidenced in Type I cumulate dunites by clinopyroxene with higher Mg# than coexisting olivine and traceelement signatures indicative of interaction with boniniticlike melts derived from refractory mantle sources.

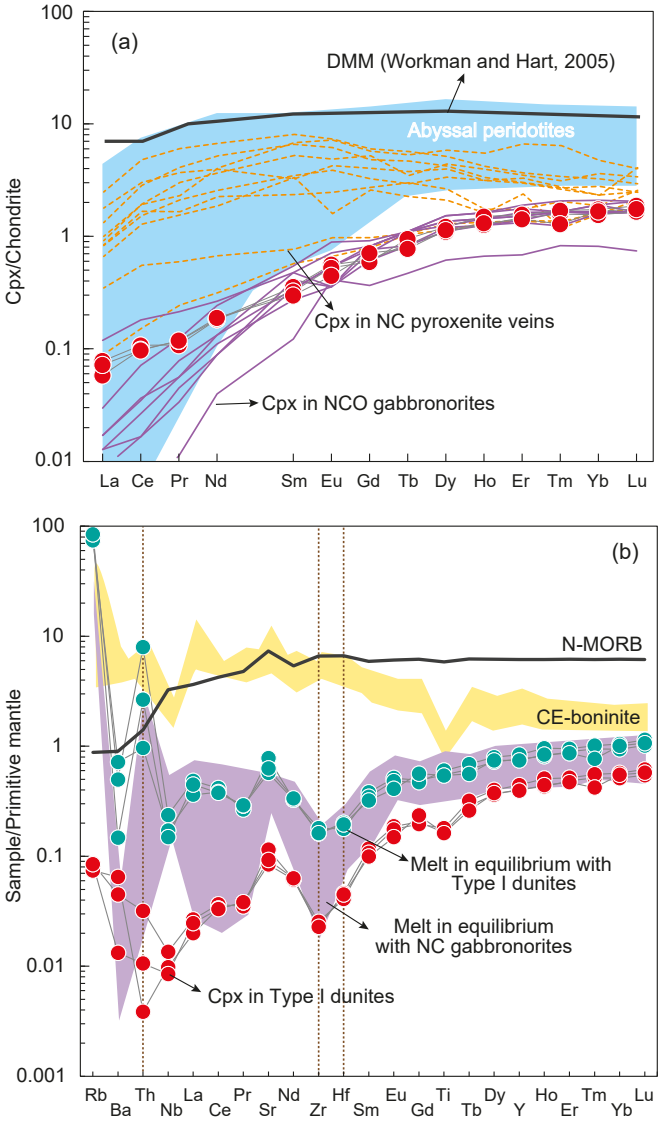

Fig. 8 - Chondrite-normalized rare earth element (REE) and primitive mantle-normalized trace element patterns of clinopyroxenes from type I dunites. Normalization values are from Anders and Grevesse (1989) and Sun and McDonough (1989). Data for depleted MORB mantle (DMM; Workman and Hart, 2005), clinopyroxene from New Caledonia pyroxenite veins (Xu et al., 2021; Secchiari et al., 2022), and gabbronorites (Secchiari et al., 2018) are shown for comparison in (a). The compositions of melts in equilibrium with clinopyroxene were calculated using partition coefficients from Sun and Liang (2012) and Adam and Green (2006). Compositions of N-MORB (Sun and McDonough, 1989), New Caledonia CE-boninites (Cluzel et al., 2016), and melts in equilibrium with gabbronorites (Secchiari et al., 2018) are provided for comparison in (b).

Table 5 - Representative trace element compositions of clinopyroxene (in ppm) in 15NC71.

Sample	15NC71-Cpx01	15NC71-Cpx02	15NC71-Cpx03	NIST 614
number	4	4	2	5
Ti	214	234	211	3.65
Rb	0.054	0.047	0.054	0.860
Sr	2.42	1.77	1.95	43.43
Y	1.85	2.02	1.80	0.81
Zr	0.255	0.284	0.256	1.074
Nb	0.010	0.007	0.006	0.839
Ba	0.313	0.453	0.093	3.052
La	0.018	0.014	0.017	0.719
Ce	0.065	0.059	0.059	0.814
Pr	0.010	0.010	0.011	0.749
Nd	0.083	0.083	0.086	0.901
Sm	0.052	0.048	0.044	0.779
Eu	0.031	0.029	0.025	0.756
Gd	0.122	0.117	0.140	0.808
Tb	0.031	0.035	0.028	0.712
Dy	0.267	0.295	0.276	0.758
Ho	0.071	0.083	0.073	0.763
Er	0.233	0.248	0.226	0.749
Tm	0.038	0.041	0.031	0.748
Yb	0.252	0.282	0.272	0.843
Lu	0.040	0.046	0.042	0.793
Hf	0.014	0.013	0.014	0.701
Th	0.0027	0.0003	0.0009	0.771

ACKNOWLEDGEMENTS

This study received financial support from the National Science Fund for Distinguished Young Scholars (42025201), the National Natural Science Foundation of China (42376063), and Laoshan Laboratory (LSKJ202502700). We thank Editor Alessandra Montanini for handling the manuscript and extend our sincere appreciation to Giulio Borghini and an anonymous reviewer for their constructive feedback, which greatly improved the paper. We are also indebted to Dominique Cluzel, Fu-Yuan Wu, Yang Chu, Wen-Bin Ji, and Qing-Ren Meng for their field assistance.

REFERENCES

Adam J., Green T., 2006. Trace element partitioning between mica- and amphibole-bearing garnet lherzolite and hydrous basanitic melt: 1. Experimental results and the investigation of controls on partitioning behaviour. Contrib. Mineral. Petrol., 152(1): 1-17. https: //doi.org/10.1007/s00410-006-0085-4

Aitchison J.C., Clarke G.L., Meffre S., Cluzel D., 1995. Eocene arc-continent collision in New Caledonia and implications for regional southwest Pacific tectonic evolution. Geology, 23(2): 161. https: //doi.org/10.1130/0091-7613(1995)023<0161: eaccin>2.3.co;2

Anders E., Grevesse N., 1989. Abundances of the elements: Meteoritic and solar. Geochim. Cosmochim. Acta., 53(1): 197-214. https: //doi.org/10.1016/0016-7037(89)90286-X

Anonymous, 1972. Penrose field conference on ophiolites. Geotimes 17.

Arai S., 1994. Characterization of spinel peridotites by olivine-spinel compositional relationships: Review and interpretation. Chem Geol, 113(3-4): 191-204. https: //doi.org/10.1016/0009-2541(94)90066-3

Arai S., Okamura H., Kadoshima K., Tanaka C., Suzuki K., Ishimaru S., 2011. Chemical characteristics of chromian spinel in plutonic rocks: Implications for deep magma processes and discrimination of tectonic setting. Island Arc, 20(1): 125-137. https: //doi.org/10.1111/j.1440-1738.2010.00747.x

Avias J., 1967. Overthrust structure of the main ultrabasic New Caledonian massives. Tectonophysics, 4(4-6): 531-541. https: //doi.org/10.1016/0040-1951(67)90017-0

Barnes S.J., Roeder P.L., 2001. The range of spinel compositions in terrestrial mafic and ultramafic rocks. J. Petrol., 42(12): 2279-2302. https: //doi.org/10.1093/petrology/42.12.2279

Basch V., Rampone E., Crispini L., Ferrando C., Ildefonse B., Godard M., 2019. Multi-stage reactive formation of troctolites in slow-spreading oceanic Lithosphere (Erro-Tobbio, Italy): a combined field and petrochemical study. J. Petrol., 60(5): 873-906. https: //doi.org/10.1093/petrology/egz019

Bédard J.H., 2010. Parameterization of the Fe= Mg exchange coefficient (Kd) between clinopyroxene and silicate melts. Chem. Geol., 274(3-4): 169-176. https: //doi.org/10.1016/j.chemgeo.2010.04.003

Beyer E.E., Griffin W.L., O'Reilly S.Y., 2006. Transformation of Archaean Lithospheric mantle by refertilization: evidence from exposed peridotites in the Western Gneiss Region, Norway. J. Petrol., 47(8): 1611-1636. https: //doi.org/10.1093/petrology/egl022

Bilici Ö., 2022. Reactive harzburgite and ultimate dunite formation as a result of boninite-like melt interaction: Petrological evidence from the Kırdağ ophiolite (Erzurum, NE Turkey). J. Afr. Earth. Sci., 193: 104601. https: //doi.org/10.1016/j.jafrearsci.2022.104601

Borghini G., Francomme J.E., Fumagalli P., 2018. Melt-dunite interactions at 0.5 and 0.7 GPa: experimental constraints on the origin of olivine-rich troctolites. Lithos, 323: 44-57. https: //doi.org/10.1016/j.Lithos,.2018.09.022

Braun M.G., Kelemen P.B., 2002. Dunite distribution in the Oman ophiolite: Implications for melt flux through porous dunite con-

duits. Geochem. Geophys. Geosyst., 3(11): 1-21. https: //doi.org/10.1029/2001GC000289

Clarke G.L., Aitchison J.C., Cluzel D., 1997. Eclogites and Blueschists of the Pam Peninsula, NE New Caledonia: a Reappraisal. J. Petrol., 36(7): 843-876. https: //doi.org/10.1093/petroj/38.7.843

Cluzel D., Aitchison J.C., Picard C., 2001. Tectonic accretion and underplating of mafic terranes in the Late Eocene intraoceanic fore-arc of New Caledonia (Southwest Pacific): geodynamic implications. Tectonophysics, 340(1-2): 23-59. https: //doi.org/10.1016/S0040-1951(01)00148-2

Cluzel D., Meffre S., Maurizot P., Crawford AJ, 2006. Earliest Eocene (53Ma) convergence in the Southwest Pacific: evidence from pre-obduction dikes in the ophiolite of New Caledonia. Terra Nova, 18(6): 395-402. https: //doi.org/10.1111/j.1365-3121.2006.00704.x

Cluzel D., Ulrich M., Jourdan F., Meffre S., Paquette J.L., Audet M.A., Secchiari A, Maurizot P, 2016. Early Eocene clinoenstatite boninite and boninite-series dikes of the ophiolite of New Caledonia; a witness of slab-derived enrichment of the mantle wedge in a nascent volcanic arc. Lithos, 260: 429-442. https: //doi.org/10.1016/j.Lithos,.2016.04.031

Cluzel D., Montanini A. Secchiari E. Ferrari M. Heizler F. Jourdan S., Meffre R. Zhou C. Teyssier C., 2024. New geochemical and age ($^{40}Ar/^{39}Ar$ and U-Pb) constraints on forearc intrusive rocks from New Caledonia Ophiolite; diversity of melts generated at hot (transcurrent) subduction inception. J. Geol. Soc. 181, jgs2023-145, ISSN: 0016-7649, doi: 10.1144/jgs2023-145

Crawford A.J., Falloon T.J., Green D.H., 1989. Classification, petrogenesis and tectonic setting of boninites. In: Crawford AJ (Ed). Boninites, Unwin Hyman, London, 1-49.

Dare S.A.S., Pearce J.A., McDonald I., Styles M.T., 2009. Tectonic discrimination of peridotites using fO2-Cr# and Ga-Ti-FeIII systematics in chrome-spinel. Chem. Geol., 261(3-4): 199-216. https: //doi.org/10.1016/j.chemgeo.2008.08.002

Dewey J.F., Bird J.M., 1971. Origin and Emplacement of the Ophiolite Suite: Appalachian Ophiolites in Newfoundland. J. Geophys. Res., 76(14): 3179-3206. https: //doi.org/10.1029/JB076i014p03179

Dick H.J.B., Bullen T., 1984. Chromian spinel as a petrogenetic indicator in abyssal and alpine-type peridotites and spatially associated lavas. Contrib. Mineral. Petrol., 86(1): 54-76. https: //doi.org/10.1007/BF00373711

Dilek Y., Furnes H., 2014. Ophiolites and their origins. Elements, 10(2): 93-100. https: //doi.org/10.2113/gselements.10.2.93

Escartín J., Canales J.P., 2011. Detachments in Oceanic Lithosphere: Deformation, Magmatism, Fluid Flow, and Ecosystems. Eos Transactions American Geophysical Union 92(4): 31-31. https: //doi.org/10.1029/2011EO040003

Fitzherbert J.A., Clarke G.L., Powell R., 2005. Preferential retrogression of high- P metasediments and the preservation of blueschist to eclogite facies metabasite during exhumation, Diahot terrane, NE New Caledonia. Lithos, 83(1-2): 67-96. https: //doi.org/10.1016/j.Lithos,.2005.01.005

Gass I.G., 1968. Is the Troodos massif of Cyprus a fragment of Mesozoic ocean floor? Nature, 220(5162): 39-42. https: //doi.org/10.1038/220039a0

Griffin W.L., Powell W.J., Pearson N.J., O'Reilly S.Y., 2008. GLITTER: data reduction software for laser ablation ICP-MS. In: Sylvester P (Ed) Laser Ablation-ICP-MS in the Earth Sciences: Current Practices and Outstanding Issues: Mineralogical Association of Canada Short Course Series, vol., 308-311.

Hattori K.H., Guillot S., Saumur B.-M., Tubrett M.N., Vidal O., Morfin S., 2010. Corundum-bearing garnet peridotite from northern Dominican Republic: A metamorphic product of an arc cumulate in the Caribbean subduction zone. Lithos, 114(3): 437-450. https: //doi.org/10.1016/j.Lithos,.2009.10.010

Herzberg C., 2004. Geodynamic information in peridotite petrology. J. Petrol., 45(12): 2507-2530. https: //doi.org/10.1093/petrology/egh039

Kelemen P.B., Johnson K.T.M., Kinzler R.J., Irving A.J., 1990. High-field-strength element depletions in arc basalts due to mantle-magma interaction. Nature, 345(6275): 521-524. https: //doi.org/10.1038/345521a0

Kelemen P.B., Shimizu N., Salters V.J.M., 1995. Extraction of mid-ocean-ridge basalt from the upwelling mantle by focused flow of melt in dunite channels. Nature, 375(6534): 747-753. https: //doi.org/10.1038/375747a0

Kinzler R.J., 1997. Melting of mantle peridotite at pressures approaching the spinel to garnet transition: Application to mid-ocean ridge basalt petrogenesis. J. Geophys. Res. Solid Earth, 102(B1): 853-874. https: //doi.org/10.1029/96JB00988

Kubo K., 2002. Dunite Formation Processes in Highly Depleted Peridotite: Case Study of the Iwanaidake Peridotite, Hokkaido, Japan. J. Petrol., 43(3): 423-448. https: //doi.org/10.1093/petrology/43.3.423

Le Roux V., Dick H.J.B., Shimizu N., 2014. Tracking flux melting and melt percolation in supra-subduction peridotites (Josephine ophiolite, USA). Contrib. Mineral. Petrol., 168: 1-22. https: //doi.org/10.1007/s00410-014-1064-9

Liu C.-Z., Xu Y., Wu F.-Y., 2018. Limited recycling of crustal osmium in forearc mantle during slab dehydration. Geology, 46(3): 239-242. https: //doi.org/10.1130/G39869.1

Liang Y., Schiemenz A., Hesse M.A., Parmentier E.M., 2011. Waves, channels, and the preservation of chemical heterogeneities during melt migration in the mantle. Geophys. Res. Lett., 38(20). https: //doi.org/10.1029/2011GL049034

Marchesi C., Garrido C.J., Godard M., Belley F., Ferré E., 2009. Migration and accumulation of ultra-depleted subduction-related melts in the Massif du Sud ophiolite (New Caledonia). Chem. Geol., 266(3-4): 171-186. https: //doi.org/10.1016/j.chemgeo.2009.06.004

Moores E.M., Vine F.J., 1971. The Troodos Massif, Cyprus and other ophiolites as oceanic crust: evaluation and implications. Philosophical Transactions of the Royal Society of London Series A, Mathematical and Physical Sciences, 268(1192): 443-467. https: //doi.org/10.1098/rsta.1971.0006

Niu Y., 1997. Mantle Melting and Melt Extraction Processes beneath Ocean Ridges: Evidence from Abyssal Peridotites. J. Petrol., 38(8): 1047-1074. https: //doi.org/10.1093/petroj/38.8.1047

Ozawa K., 1994. Melting and melt segregation in the mantle wedge above a subduction zone: evidence from the chromite-bearing peridotites of the Miyamori ophiolite complex, northeastern Japan. J. Petrol., 35(3): 647-678. https: //doi.org/10.1093/petrology/35.3.647

Parkinson I.J., Pearce J.A., 1998. Peridotites from the Izu-Bonin-Mariana Forearc (ODP Leg 125): Evidence for Mantle Melting and Melt-Mantle Interaction in a Supra-Subduction Zone Setting. J. Petrol., 39(9): 1577-1618. https: //doi.org/10.1093/petroj/39.9.1577

Pearce J.A., Reagan M.K., 2019. Identification, classification, and interpretation of boninites from Anthropocene to Eoarchean using Si-Mg-Ti systematics. Geosphere, 15(4): 1008-1037. https: //doi.org/10.1130/GES01661.1

Pirard C., Hermann J., O'Neill H.S.C., 2013. Petrology and Geochemistry of the Crust-Mantle Boundary in a Nascent Arc, Massif du Sud Ophiolite, New Caledonia, SW Pacific. J. Petrol., 54: 1759-1792. https: //doi.org/10.1093/petrology/egt030

Prinzhofer A., Allègre C.J., 1985. Residual peridotites and the mechanisms of partial melting. Earth Planet Sci. Lett., 74(2-3): 251-265. https: //doi.org/10.1016/0012-821X(85)90025-1

Roeder P.L., Emslie R.F.l., 1970. Olivine-liquid equilibrium. Contrib. Mineral. Petrol., 29(4): 275-289. https: //doi.org/10.1007/BF00371276

Rollinson H., 2019. Dunites in the mantle section of the Oman ophiolite-The boninite connection. Lithos, 334: 1-7. https: //doi.org/10.1016/j.Lithos,.2019.03.008

Saccani E., Tassinari R., 2015. The role of MORB and SSZ magmatypes in the formation of Jurassic ultramafic cumulates in the Mirdita ophiolites (Albania) as deduced from chromian spinel and olivine chemistry. Ofioliti, 40(1): 37-56. https: //dx.doi.org/10.4454/ofioliti.v40i1.434

Saka S., Uysal I., Akmaz R.M., Kaliwoda M., Hochleitner R., 2014. The effects of partial melting, melt-mantle interaction and fractionation on ophiolite generation: Constraints from the late Cretaceous Pozantı-Karsantı ophiolite, southern Turkey. Lithos, 202: 300-316. https: //doi.org/10.1016/j.Lithos,.2014.05.027

Sanfilippo A., Tribuzio R., Ottolini L., Hamada M., 2017. Water, lithium and trace element compositions of olivine from Lanzo South replacive mantle dunites (Western Alps): New constraints into melt migration processes at cold thermal regimes. Geochim. Cosmochim. Acta., 214: 51-72. https: //doi.org/10.1016/j.gca.2017.07.034

Santos J.F., Schärer U., Gil Ibarguchi J.I., Girardeau J., 2002. Genesis of pyroxenite-rich peridotite at Cabo Ortegal (NW Spain): geochemical and Pb-Sr-Nd isotope data. J. Petrol., 43(1): 17-43. https: //doi.org/10.1093/petrology/43.1.17

Secchiari A., Montanini A., Bosch D., Macera P., Cluzel D., 2016. Melt extraction and enrichment processes in the New Caledonia lherzolites: Evidence from geochemical and Sr-Nd isotope data. Lithos, 260: 28-43. https: //doi.org/10.1016/j.Lithos,.2016.04.030

Secchiari A., Montanini A., Bosch D., Macera P., Cluzel D., 2018. The contrasting geochemical message from the New Caledonia gabbronorites: insights on depletion and contamination processes of the sub-arc mantle in a nascent arc setting. Contrib. Mineral. Petrol., 173(8): 66. https: //doi.org/10.1007/s00410-018-1496-8

Secchiari A., Montanini A., Bosch D., Macera P., Cluzel D., 2019. Origin of the spinel-pyroxene symplectites in the harzburgites from the New Caledonia Peridotite. Ofioliti, 44(1): 31-42. https: //doi.org/10.4454/ofioliti.v44i1.463

Secchiari A., Montanini A., Bosch D., Macera P., Cluzel D., 2020. Sr, Nd, Pb and trace element systematics of the New Caledonia harzburgites: Tracking source depletion and contamination processes in a SSZ setting. Geosci. Front., 11(1): 37-55. https: //doi.org/10.1016/j.gsf.2019.04.004

Secchiari A., Montanini A., Cluzel D., 2022. Hydrous mafic-ultramafic intrusives at the roots of a proto-arc: implications for crust building and mantle source heterogeneity in young forearc regions. Contrib. Mineral. Petrol., 177(4): 50. https: //doi.org/10.1007/s00410-022-01912-x

Su B., Chen Y., Guo S., Liu J., 2016. Origins of orogenic dunites: Petrology, geochemistry, and implications. Gondwana. Res., 29(1): 41-59. https: //doi.org/10.1016/j.gr.2015.08.001

Suhr G., Hellebrand E., Snow J.E., Seck H.A., Hofmann A.W., 2003. Significance of large, refractory dunite bodies in the upper mantle of the Bay of Islands Ophiolite. Geochem. Geophys. Geosyst., 4(3) https: //doi.org/10.1029/2001GC000277

Suhr G., Seck H.A., Shimizu N., Günther D., Jenner G., 1998. Infiltration of refractory melts into the lowermost oceanic crust: evidence from dunite-and gabbro-hosted clinopyroxenes in the Bay of Islands Ophiolite. Contrib. Mineral. Petrol., 131(2): 136-154. https: //doi.org/10.1007/s004100050384

Sun C., Liang Y., 2012. Distribution of REE between clinopyroxene and basaltic melt along a mantle adiabat: effects of major element composition, water, and temperature. Contrib. Mineral. Petrol., 163: 807-823. https: //doi.org/10.1007/s00410-011-0700-x

Sun S.S., Mcdonough W.F., 1989. Chemical and isotopic systematics of oceanic basalts: implications for mantle composition and processes. Geol Soc, London, Special Publications, 42(1): 313-345. https: //doi.org/10.1144/GSL.SP.1989.042.01.19

Ulmer P., Kaegi R., Müntener O., 2018. Experimentally derived intermediate to silica-rich arc magmas by fractional and equilibrium crystallization at 1· 0 GPa: an evaluation of phase relationships, compositions, liquid lines of descent and oxygen fugacity. J. Petrol., 59(1): 11-58. https: //doi.org/10.1093/petrology/egy017

Ulrich M., Picard C., Guillot S., Chauvel C., Cluzel D., Meffre S., 2010. The New Caledonia Ophiolite: Multiple melting stages and refertilisation process as indicators for ridge to subduction formation. Lithos, 115(1): 223-236. https: //doi.org/10.1016/j.Lithos,.2009.12.011

Walter M.J., 1998. Melting of garnet peridotite and the origin of komatiite and depleted Lithosphere. J. Petrol., 39(1): 29-60. https: //doi.org/10.1093/petroj/39.1.29

Warren J.M., 2016. Global Variations in Abyssal Peridotite Compositions. Lithos, 248-251: 193-219. https: //doi.org/10.1016/j.lithos.2015.12.023

Workman R.K., Hart S.R., 2005. Major and trace element composition of the depleted MORB mantle (DMM). Earth Planet Sci. Lett., 231(1-2): 53-72. https: //doi.org/10.1016/j.epsl.2004.12.005

Xie Z., Hattori K., Wang J., 2013. Origins of ultramafic rocks in the Sulu Ultrahigh-pressure Terrane, Eastern China. Lithos, 178: 158-170. https: //doi.org/10.1016/j.Lithos,.2012.12.003

Xiong Q., Henry H., Griffin W.L., Zheng J.-P., Satsukawa T., Pearson N.J., O'Reilly S.Y., 2017. High-and low-Cr chromitite and dunite in a Tibetan ophiolite: evolution from mature subduction system to incipient forearc in the Neo-Tethyan Ocean. Contrib. Mineral. Petrol., 172(6): 45. https: //doi.org/10.1007/s00410-017-1364-y

Xiong Q., Xu Y., González-Jiménez J.M., Liu J., Alard O., Zheng J.-P., Griffin W.L., O'Reilly S.Y., 2020. Sulfide in dunite channels reflects long-distance reactive migration of mid-ocean-ridge melts from mantle source to crust: A Re-Os isotopic perspective. Earth Planet Sci. Lett., 531: 115969. https: //doi.org/10.1016/j.epsl.2019.115969

Xu Y., Liu C.-Z., 2019. Subduction-induced fractionated highly siderophile element patterns in forearc mantle. Minerals, 9(6): 339. https: //doi.org/10.3390/min9060339

Xu Y., Liu C.Z., Lin W., 2021. Melt extraction and reaction in the forearc mantle: Constraints from trace elements and isotope geochemistry of ultra-refractory peridotites of the New Caledonia Peridotite Nappe. Lithos, 380-381: 105882. https: //doi.org/10.1016/j.Lithos,.2020.105882

Xu Y., Liu C.Z., Lin W., Shi X.F., 2022. Ancient depletion signals in lherzolites from forearc region: Constraints from Lu-Hf isotope compositions. Geosci. Front., 13(1): 101259. https: //doi.org/10.1016/j.gsf.2021.101259

Xu Y., Liu C.-Z., Lin Y.-Z., Liu B.-D., 2025. Crust-mantle decoupling in the Gakkel Ridge induced by strong heterogeneity of the asthenosphere. Contrib. Mineral. Petrol., 180(2): 13. https: //doi.org/10.1007/s00410-025-02198-5

Xu Y., Liu C.-Z., Shi X.-F., 2024. Ancient melt percolation in forearc mantle pyroxenites: Evidence from highly siderophile elements and Os isotope ratios. Geochim. Cosmochim. Acta., 374: 173-185. https: //doi.org/10.1016/j.gca.2024.04.031

Xu Y., Liu C.-Z., Shi X.-F., Lin W., 2022. Petrogenesis of Eocene mafic and felsic magmas in the New Caledonia ophiolite: geochemistry and geochronology constraints. Int. Geol. Rev., 64(15): 2186-2203. https: //doi.org/10.1080/00206814.2021.1978111

Zhang C., Liu C.-Z., Bénard A., Müntener O., Ji W.-B., Liu T., Zhang Z.-Y., Zhang W.-Q., Wu F.-Y., 2023. Heterogeneous mantle beneath the Neo-Tethys Ocean revealed by ultramafic rocks from the Xiugugabu Ophiolite in the Yarlung-Tsangpo Suture Zone, southwestern Tibet. Contrib. Mineral. Petrol., 178(8): 54. https: //doi.org/10.1007/s00410-023-02039-3

Zhou M., Robinson P.T., Malpas J., Edwards S.J., Qi L., 2005. REE and PGE Geochemical Constraints on the Formation of Dunites in the Luobusa Ophiolite, Southern Tibet. J. Petrol., volume 46(3): 615-639. https: //doi.org/10.1093/petrology/egh091

Zhou X., Zheng J.P., Li Y., Zhu H., Griffin W.L., O'Reilly S.Y., 2021. Melt migration and interaction in a dunite channel system within oceanic forearc mantle: the Yushigou harzburgite-dunite associations, North Qilian ophiolite (NW China). J. Petrol., 62(7): egaa115. https://doi.org/10.1093/petrology/egaa115

Received, October 22, 2025;
Accepted, December 22, 2025